The Effects of Shear Parameters on Dynamic Response Behavior of EEM based on Numerical Simulation

Jianmin Zhou, Yongsheng Jia*, Mingsheng Zhao, Xuelai Shu

Abstract—**The dynamic response behavior of the emulsion explosive matrix (EEM) during the shearing process was investigated using the ANSYS-Fluent numerical analysis method. The effects of shear parameters on the flow field distribution, shear rate, and mixing time of EEM were systematically analyzed. The results indicated that the turbine blade exerts the most significant influence on the flow characteristics of EEM. As the blade length and the number of blade layers increase, both the turbulent range and velocity of EEM also increase. Specifically, the shear rate generated by the turbine blade is the highest, followed by the push blade and the paddle blade. With increasing blade length, the impact of the blade on the vortex formation of the fluid near the wall becomes more pronounced, leading to a continuous increase in wall shear stress and shear range. Additionally, as the blade length increases, the radial stirring effect of the blade on EEM becomes more evident, accompanied by an increase in turbulent kinetic energy. Increasing the number of blade layers enhances the vortex flow of EEM, resulting in a significant increase in the turbulent region. Furthermore, as the blade length and the number of blade layers increase, the mixing time of EEM decreases, with the push paddle achieving the shortest mixing time.**

Index Terms—**EEM, numerical simulation, shear parameters, dynamic response, parameter optimization**

I. Introduction

Shear stirring has been extensively utilized in the chemical industry. Extensive practical experience indicates that the optimal shear stirring process involves preparing uniformly mixed, free-flowing, and highly stable EEM within the shortest time frame while minimizing power consumption [1-3]. To ensure the stability of EEM preparation, apart from maintaining feed stability, the most critical parameter is shear stirring. Alterations in the geometric dimensions and shapes of shear blades significantly influence the shear action on the surrounding fluid and can substantially modify the shear mixing process and rheological properties of materials [4-7].

In recent years, computational fluid dynamics (CFD)-based predictive technology has been increasingly applied to agitator design, effectively addressing certain limitations [8-11]. The CFD method has been widely employed in studies of solid-liquid and gas-liquid mixing and separation, such as in stirring tanks and cyclones, to determine the critical speed of solid particles in solid-liquid two-phase flows and investigate the effects of stirring paddle structure and solid phase concentration on stirred mixing flow fields [12-18]. By comparing simulation results with experimental data, optimized multi-zone model parameters for calculating population balance equations have been obtained. Despite numerous studies using the CFD method to simulate mixing processes in stirred tanks, comprehensive analyses of flow field velocity, shear rate, and mixing time remain under-reported.

In this study, the ANSYS-Fluent numerical analysis method was employed to investigate the dynamic response behavior of EEM during the shear process. By varying shear parameters, including blade shape, length, and number of blade layers, the flow field distribution, shear rate, and mixing efficiency during shear process of EEM were analyzed. Ultimately, the optimal shear stirring parameters for EEM were determined.

II. ANSYS-Fluent Numerical Analysis Method

A. Turbulent Flow of EEM Fluid and Its Algorithm

The shear stirring process of EEM is non-steady-state, and the dispersion of EEM droplets is achieved through intense shear stirring. Therefore, the shear stirring process of EEM mainly exhibits turbulent motion. Considering the motion behavior of EEM stirring process, the RNG k-ε model is selected to calculate the turbulent flow problem of EEM shear stirring process. This model fully considers the vortices in EEM flow process and can better conform to the shear stirring process of EEM. The kinetic energy and diffusion equations of the RNG k-ε model are shown in the following formulas.

$$\frac{\partial(\rho k)}{\partial t}+\frac{\partial(\rho k u_i)}{\partial x_i}=\frac{\partial\left[\alpha_k u_{eff}\frac{\partial k}{\partial x_i}\right]}{\partial x_i}+G_k+G_b-\rho\varepsilon-Y_M+S_K \quad (1)$$

$$\frac{\partial(\rho \varepsilon)}{\partial t}+\frac{\partial(\rho k u_i)}{\partial x_i}=\frac{\partial\left[\alpha_\varepsilon u_{eff}\frac{\partial \varepsilon}{\partial x_j}\right]}{\partial x_j}+C_{1\varepsilon}\frac{\varepsilon}{k}(G_k+C_{3\varepsilon}G_b)-C_{2\varepsilon}\rho\frac{\varepsilon^2}{k}+S_c \quad (2)$$

Where, u_i is time mean velocity; u_{eff} is effective viscosity coefficient; α_k is the effective turbulent pelant

Manuscript received January 13, 2025; revised June 12, 2025.

This work was supported by the [State Key Laboratory of Precision Blasting and Hubei Key Laboratory of Blasting Engineering, Jianghan University] under Grant [PBSKL2022C02] and [National Natural Science Foundation of China] under Grant [52064003].

Jianmin Zhou is a senior engineer of State Key Laboratory of Precision Blasting, Jianghan University, Wuhan, 430056 China (e-mail: zjm377413454@126.com).

Yongsheng Jia is a professor of State Key Laboratory of Precision Blasting, Jianghan University, Wuhan, 430056 China (phone: 13628618896; fax: 073185092908; e-mail: 609991197@qq.com).

Mingsheng Zhao is a professor of University of Guizhou, Guiyang, 550001 China (e-mail: 514416902@qq.com).

Xuelai Shu is an engineer of Hongda Blasting Engineering Group, Co., Ltd. Changsha, 410001 China (e-mail: 468174266@qq.com).

coefficient; ρ is the viscosity coefficient of turbulence; ε is the dynamic viscosity of the oil phase; G_b is the production term of turbulent energy k caused by fluid buoyancy; G_k is the turbulent energy k generated by the velocity gradient.

$$G_k = u_i \left(\frac{\partial (u_i)}{\partial x_j} + \frac{\partial (u_j)}{\partial x_i} \right) \frac{\partial (u_i)}{\partial x_j} \quad (3)$$

Where, $C_{1\varepsilon}$, $C_{2\varepsilon}$, $C_{3\varepsilon}$ are the constant coefficient, in RNG k-ε model, $C_{1\varepsilon}$ is 1.42, $C_{2\varepsilon}$ is 1.68, $C_{3\varepsilon}$ is 0; Y_M is the incompressible coefficient of fluid; S_K, S_c are the custom source item.

B. Parameters Setting of Fluid Model Calculation

The single-phase model is used to simulate the velocity field of EEM, and the two-phase model is used to simulate the concentration field. The simulation environment is set at 1 ATM in this paper. After the initialization of the concentration field simulation, the patch function is used to set the initial concentration of the tracer to 1, and the initial concentration of other areas to 0. When simulating the unsteady process of EEM, the time step is set to be less than 1/10 of the reciprocal of the rotational speed. Through iterative calculations, the concentration values of EEM at different times are finally obtained to observe the mixing time.

III. Shear Parameter Setting and Simulation Modeling of EEM

A. The Structure Parameter and Fluid Parameter Setting of the Model

This paper simulates the effects of different parameter conditions (paddle type, paddle length, paddle layer number) on the flow velocity, shear rate, turbulent kinetic energy, and mixing time of EEM. The model takes a cylindrical stirring tank as the simulation object, and the simulated system is a medium-viscosity EEM. The diameter of the stirring tank is 100 mm, the height is 150 mm, and the liquid level height is 100 mm. In the initial state, the entire stirring tank is filled with EEM with non-Newtonian fluid characteristics, and its density is 1250 kg/m^3. The consistency index, power law index, yield stress and critical shear rate of EEM were set as 17.41, 0.425, 52.61 Pa and 0.001 1/s, respectively.

To accurately obtain the shear stirring flow process of EEM, this paper uses the multiple reference frame model (MRF) to simulate the steady-state stirring process in the stirring tank. The stirring tank model is divided into two regions: the moving region and the stationary region. The moving region is a virtual region with a cylindrical shape and is slightly larger than the paddle length, while the stationary region is all the flow areas except the moving region. The stirring speed of all working conditions is set to 1200 rpm.

To accurately predict the mixing time of the stirring and mixing process, monitoring points are set at multiple positions in the stirring tank to observe the change process of the tracer concentration at each monitoring point over time. When the tracer concentrations at multiple monitoring points reach a stable state, it is considered that EEM has reached the uniform mixing time. After the single-phase fluid calculation converges, the fluid transient simulation is performed by adding a tracer. The density of the tracer is 1186 kg/m^3, and the viscosity is 2.3*10^{-3} Pa.s.

In this paper, three monitoring points are set at the free surface F1, the middle F2, and the bottom F3 of the stirring tank to monitor the concentration. The coordinates of F1 are all (-0.025, 0, 0.095), those of F3 are all (0.045, 0, 0.005), and the coordinates of single-layer blade F2 are (0.045, 0, 0.05). P1 is the tracer feed point, with its coordinate values being (0.035, 0, 0.095), and the diameter of the tracer addition is set at 0.01 m. Different monitoring points and the tracer feed point are shown in Fig. 1.

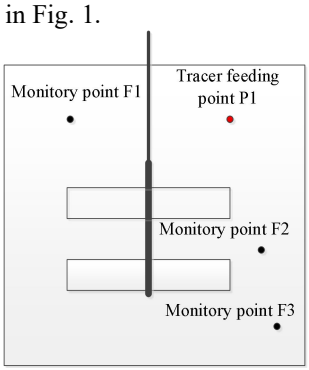

Fig. 1. Locations of different monitoring points and tracer feeding points

B. Geometric Modeling

(1) Different types of shear blades (paddle type, push type, turbine type)

All blades are single-layer, with the blade position being 50 mm above the bottom, blade length being 30 mm, the diameter of the middle cylinder being 10 mm, the diameter of the stirring tank being fixed at 100 mm, the blade width being fixed at 10 mm, and the thickness being 2 mm.

(2) Different blade lengths of shear blades

Based on the shape of paddle blades, the blade lengths are 25 mm, 30 mm, and 35 mm respectively, with the diameter of the stirring tank being fixed at 100 mm, the blade width being fixed at 10 mm, and the thickness being 2 mm.

(3) Different blade layers of shear blades

Based on the shape of paddle blades, the blade layers are 1 layer, 2 layers, and 3 layers respectively, with the layer spacing being 15 mm. The 1st layer is located at the center position of the liquid surface height (50 mm above the bottom), the positions of the 2nd layer blades are 30 mm and 60 mm above the bottom, and the positions of the 3rd layer blades are 25 mm, 50 mm, and 75 mm above the bottom. The diameter of the stirring tank is fixed at 100 mm, the blade length is fixed at 30 mm, the width is 10 mm, and the thickness is 2 mm.

C. Meshing and Boundary Condition Setting

The model is imported into the ANSYS Workbench platform, the meshing software is used to perform meshing on the stirring tank model, with the mesh type being tetrahedral mesh. The schematic diagrams of the meshes of different computational models are shown in Fig. 2.

During the simulation of the stirring process, the moving area is defined as the region rotating around the Z-axis, and the blades are set as wall boundaries with a relative rotational speed of 0 rpm to the moving area.

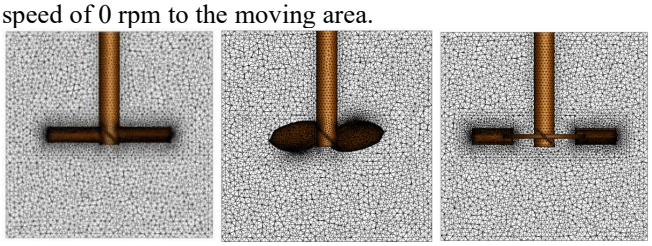

(a) paddle type (b) push type (c) turbine type

Fig. 2. The grids diagram of different calculation models

IV. Numerical Simulation Results and Analysis

A. Analysis of Flow Field Distribution and Influence of Flow Velocity on EEM

The influence of different blade types on the flow field distribution of EEM in the stirring tank is shown in Fig. 3. The results indicate that under the shear action of the stirring blades, EEM has the maximum velocity near the blades and a gradually decreasing velocity gradient trend in the axial and radial regions far from the blades. The velocity of EEM in most areas of the stirring tank changes little, and there are stirring dead zones. Among them, the paddle blade has the least shear effect on EEM, with the smallest turbulent velocity range, while the turbine blade has the largest shear effect range.

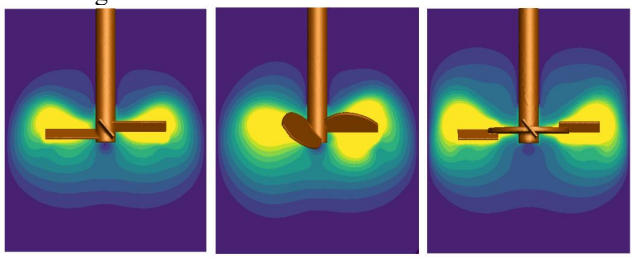

(a)paddle type (b) push type (c) turbine type

Fig.3. Influence of different blade types on flow field distribution of EEM

To further understand the velocity distribution of EEM flow field in the stirring tank, three monitoring points are set at the bottom (F1), middle (F2), and top (F3) of the stirrer to study the velocity changes, and the results are shown in Fig. 4. The results show that the fluid velocity in the middle area of the stirring blade is the largest, and the velocity distribution shows a peak-shaped trend with a high value in the middle and low values on both sides. Due to the pushing effect of the blades on the fluid, the fluid flows from the center to the wall, and at this time, there are stirring dead zones at the top and bottom of the stirring tank.The turbine blade has the greatest influence on the flow velocity of EEM, with the velocity at the F2 detection point being approximately 0.95 m/s, followed by the propeller blade, while the paddle blade has the smallest flow velocity, only about 0.15 m/s. This indicates that , the turbine blade has the strongest shear stirring effect on EEM under the same shear strength conditions.

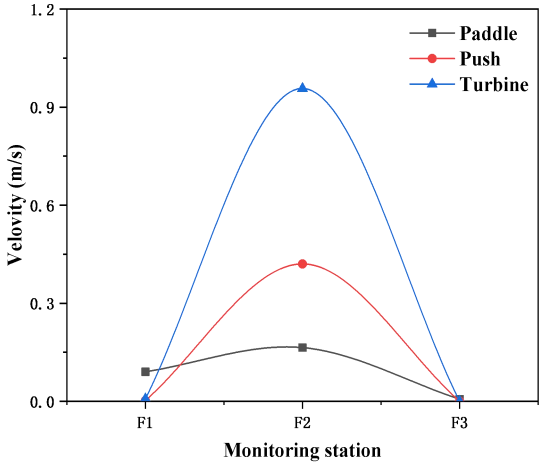

Fig. 4. Influence of blade type on velocity distribution at each monitoring point

The influence of blade length on the flow field distribution of EEM is shown in Fig. 5. The results show that the flow range of EEM increases with the increase in blade length. When the blade length is 25 mm, the stirring turbulence zone is limited to the area around the impeller. As the blade length increases, the range of the impeller's shear action on EEM in the axial and radial directions also increases. When the blade length is 35 mm, the radial stirring area of the impeller covers the entire wall, while the axial stirring area approaches the bottom of the tank.

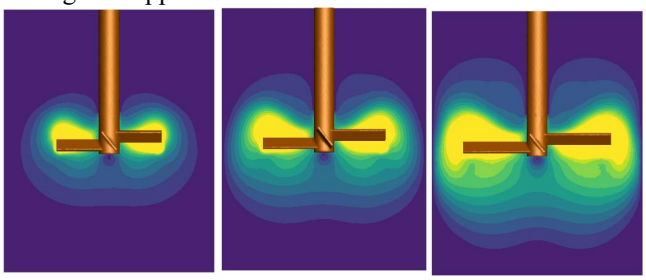

(a)25mm (b) 30mm (c) 25mm

Fig.5. Influence of blade length on flow field distribution of EEM

The influence of different blade lengths on the velocity distribution at each monitoring point in the stirring tank is shown in Fig. 6. The results indicate that as the blade length increases, the flow velocity of EEM at monitoring point F2 shows a stepwise increasing trend, and the influence of blade length on the velocity at F1 and F3 can be ignored.

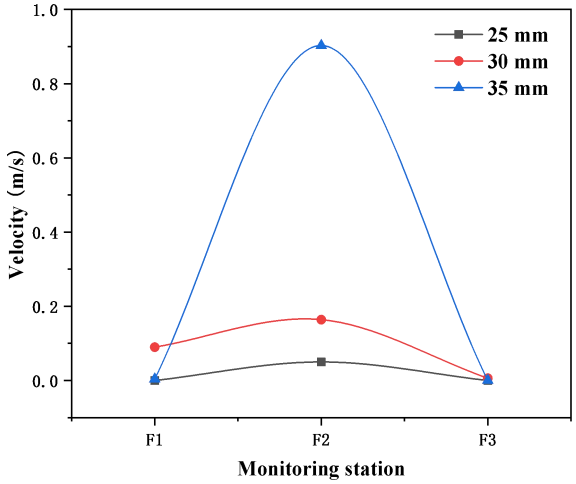

Fig.6. Influence of blade length on velocity distribution at each monitoring point

The influence of different blade layers on the flow field distribution of EEM is shown in Fig. 7. The results show that the flow range of EEM increases with the increase in the number of blade layers. When using a single-layer impeller for stirring, only a small area around the impeller is mixed. The double-layer impeller enhances the mixing intensity in the upper and bottom areas of the tank. When the number of impeller layers increases to three, the overall turbulent range of the tank increases, basically covering all the mixing areas of the tank.

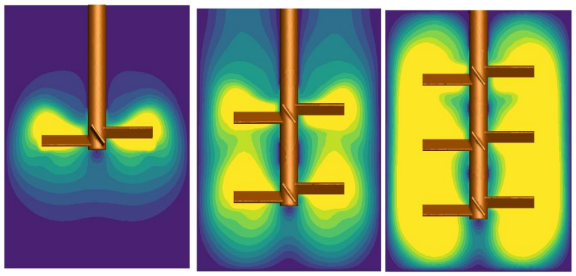

(a) one layer (b) double layers (c) three layers

Fig.7. Influence of the number of blade layers on velocity distribution

The influence of different blade layers on the velocity distribution at each monitoring point in the stirring tank is shown in Fig. 8. The results show that the flow velocity at monitoring points F1 and F2 with a double-layer impeller is significantly greater than that with a single-layer impeller, while the flow velocity of EEM at the bottom of the tank (F3) is basically the same. This indicates that although the double-layer impeller can significantly improve the stirring intensity in the upper and middle parts of the tank, the increase in the stirring intensity of EEM at the bottom of the tank is limited. Additionally, the flow velocity of EEM at F2 with both single-layer and double-layer impellers is significantly greater than that at F1, indicating that the flow intensity of EEM in the upper part of the tank is still lower than that in the middle part.

The flow velocity at the same monitoring points with three-layer impellers is the highest, and the flow velocities at the three monitoring points show a linear decreasing trend, indicating that the increase in the number of impeller layers promotes the mixing effect of EEM in the upper part of the tank.

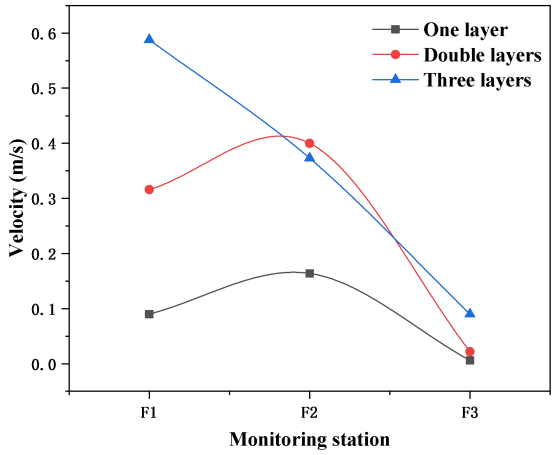

Fig.8. Influence of the number of agitator layers on the velocity at the three monitoring points

B. Analysis of the influence of shear parameters on the shear rate of EEM

The distribution curves of the shear rate along the radial direction at different heights for different impeller types are shown in Fig. 9. The results show that the radial shear rate of EEM at different heights all present a trend of being higher in the middle and lower on both sides. Meanwhile, the shear rate of EEM in the upper and lower areas of the impeller is much smaller than that in the middle area.

At the bottom of the tank (z=0.02 m), the maximum shear rate of the paddle impeller is located at the center of the stirring shaft, while the maximum shear rate of the propeller and turbine impellers is basically at the tip of the impeller. At the middle area of the tank (z=0.05 m), the turbine impeller has the highest shear rate at the same horizontal position, and the propeller impeller has the lowest. At the top of the tank (z=0.08 m), the propeller impeller has the highest shear rate, especially at the center of the stirring shaft.

The distribution curves of the shear rate along the radial direction at different heights for different blade lengths are shown in Fig. 10.

The results show that the blade length has a significant impact on the shear rate of EEM in the tank, that is, the longer the blade, the greater the shear rate of EEM. The shear rate of EEM at different heights all present a trend of being higher in the middle and lower on both sides.

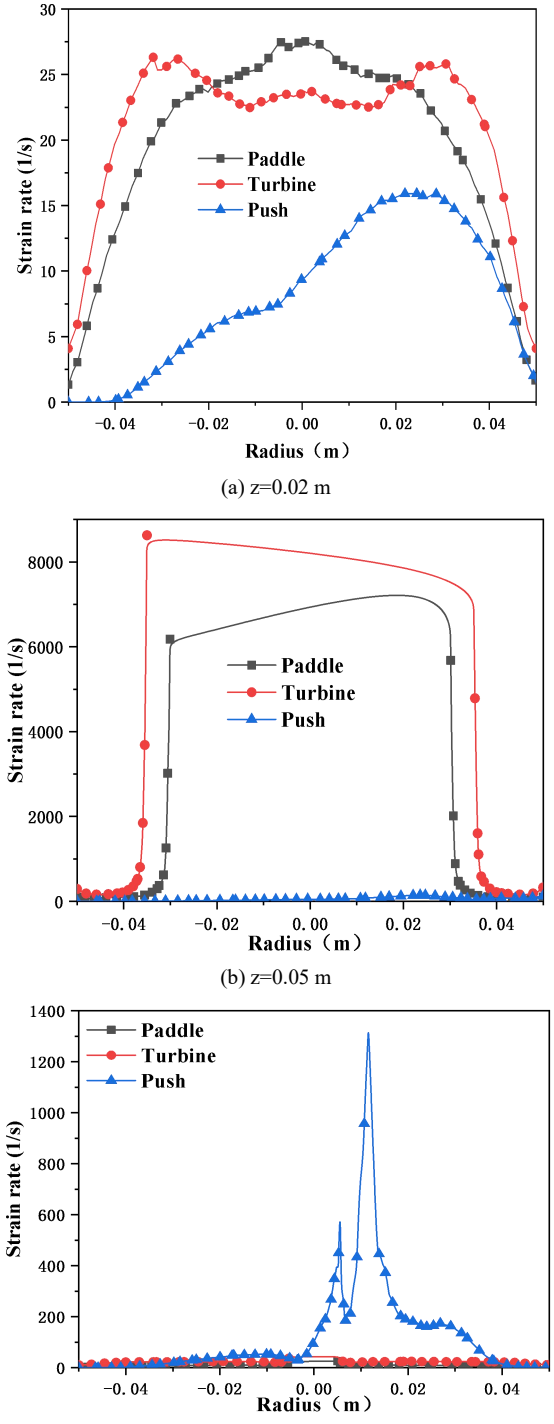

Fig.9. Radial distribution curves of shear rate of different blade types at different heights

The results show that at the upper part (z=0.02 m) and bottom (z=0.08 m) of the tank, the shear rate of EEM increases with the increase in blade length, especially at the middle position of the impeller, where EEM has a rapidly increasing high shear rate effect.

At the middle part of the tank (z=0.05 m), since the three impellers with different blade lengths have the same rotational speed, the flow velocity of EEM around the impeller is not significantly different, resulting in a basically consistent shear rate at this position. That is, the shear rate of EEM with a 35 mm blade length is slightly greater than that with a 30 mm blade length, while the shear rate of EEM with a 25 mm blade length is the smallest, but the differences among the three are slight.

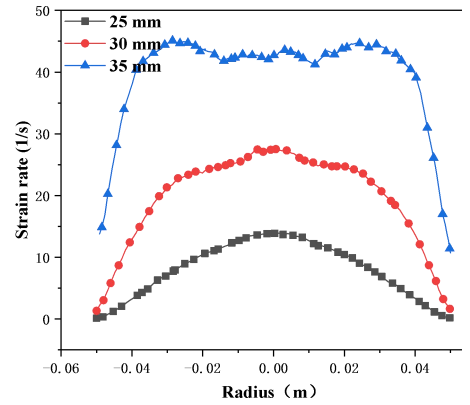

(a) z=0.02 m

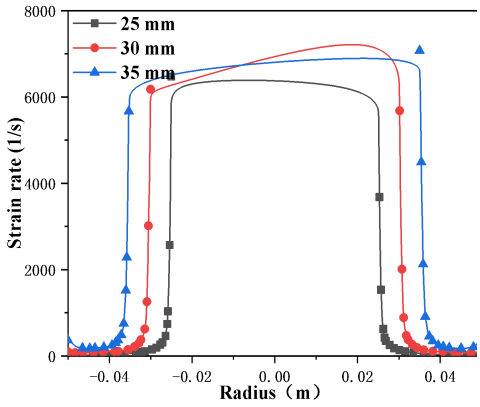

(b) z=0.05 m

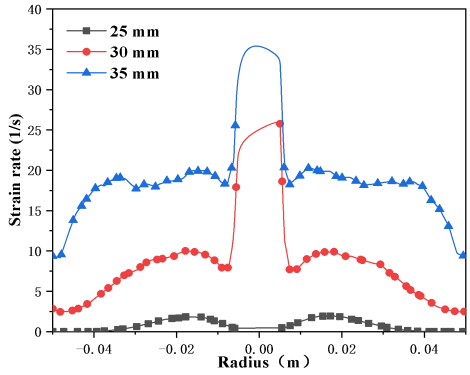

(c) z=0.08 m

Fig.10. Radial distribution curve of shear rate with different blade lengths and different heights

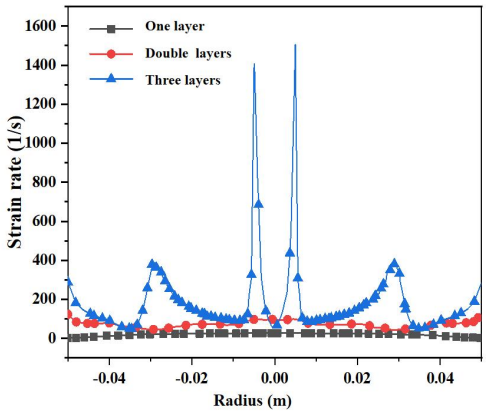

(a) z=0.02 m

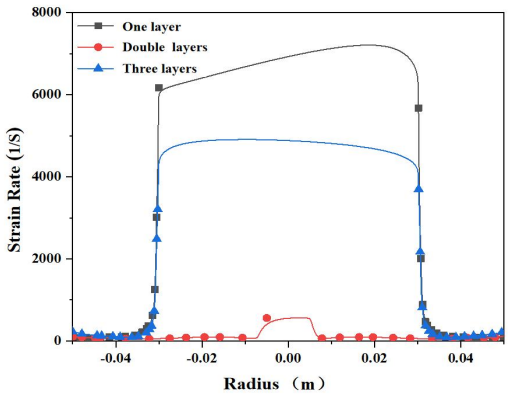

(b) z=0.05 m

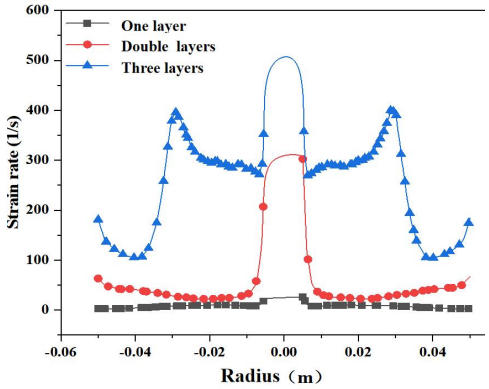

(c) z=0.08 m

Fig.11. Radial distribution of shear rate with different blade layers at different heights

The distribution curves of the shear rate of EEM under different numbers of impeller layers are shown in Fig. 11. The results indicate that the stirring range and the shear effect on EEM of multi-layer impellers are much greater than those of single-layer impellers. The shear rate of EEM shows a trend of being higher in the middle and lower on both sides at different heights.

In the upper (z = 0.08 m) and lower (z = 0.02 m) regions of the stirring tank, the shear rate of EEM increases rapidly with the increase in the number of impeller layers. However, in the middle region (z = 0.05 m) of the stirring tank, the shear rate of EEM is the highest under the single-layer impeller condition, followed by the three-layer impeller, and the shear rate is the lowest under the two-layer impeller. The reason for this is mainly that the installation positions of the two-layer and three-layer impellers are farther from the middle position of the stirring tank, resulting in a lower shear rate than that of the single-layer impeller.

C. *Analysis of Shear Mixing Uniformity of EEM*

After the flow field simulation of EEM converges, the transient simulation stage begins, and the volume-weighted mixing rule is used for the shear mixing analysis of EEM. According to Fig. 1, the tracer feed point is set at position P1. When the concentrations at the three monitoring points at the top, middle, and bottom of the stirring impeller stabilize at 95%, it is considered that the mixture is uniform, and the time taken is the stirring mixing time of EEM.

The variation curves of the tracer concentration at each monitoring point under the three-layer impeller condition over time are shown in Fig. 12. The results show that due to the differences in the positions of the monitoring points, the trends of the tracer concentration change curves at each monitoring point are different. The F1 monitoring point is located at the release height of the tracer. During the stirring process, the tracer mainly diffuses in the upper part of the

stirring tank, causing the tracer concentration at this point to continuously increase over time. After reaching the peak concentration, the tracer diffuses uniformly in the stirring tank with EEM, causing the tracer concentration at the F1 point to continuously decrease around 0.5 s and then reach a stable state. The F2 monitoring point is located at the center height position of the stirring impeller. Due to the strong stirring intensity at this position, the continuous vortex action of EEM drives the tracer to continuously move in a circular motion, causing the tracer concentration at the F2 point to reach a stable state faster than at other monitoring points. The F3 point is located at the bottom of the stirring tank where the turbulence is weak and far from the tracer release position, so the F3 monitoring point takes the longest time to reach a stable state.

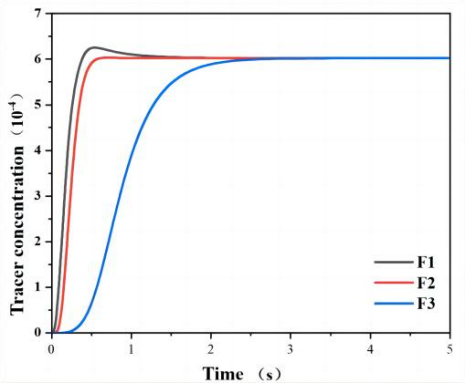

Fig.12. Tracer concentration curve with time at each monitoring point under the condition of three-layer agitator

The diffusion variation law of the tracer concentration over time under the three-layer impeller condition is shown in Fig. 13. The results show that when time is 0 s, the tracer is released at the top of the stirring tank, and the turbulent action of the impeller drives the tracer to diffuse, causing the diffusion range of the tracer to gradually increase and the concentration to be continuously diluted. When time is 0.5 s, the tracer diffuses downward with the vortex to the center position of the stirring impeller, and at this time, there is a significant gradient distribution of the tracer concentration in the stirring tank. When time is 1.5 s, the tracer is dispersed in most areas of the stirring tank, but the tracer concentration in the upper part of the stirring tank is still significantly higher than that in the bottom part. When time is 2 s, the tracer concentration in the entire stirring tank is basically uniform, and at this time, the tracer has uniformly diffused throughout the stirring tank.

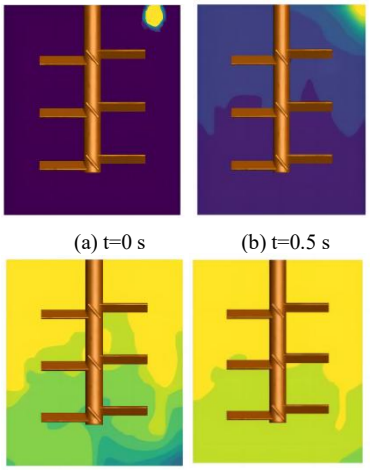

(a) t=0 s (b) t=0.5 s

(c) t=1.5 s (d) t=2 s

Fig.13. Diffusion of tracer concentration with time

The variation curves of the mixing time of EEM under different working conditions are shown in Fig. 14. As shown in Fig. 14 (a), the paddle blade and the turbine blade mainly act on the axial direction of EEM. Compared with the paddle blade, the turbine blade has a larger stirring range, and the radial movement speed of EEM on the wall of the stirring tank is greater, resulting in a stronger axial vortex generated after EEM collides with the wall of the stirring tank, making the mixing effect of the turbine blade better. Therefore, the mixing time of the propeller blade is the shortest, about 5.1 s.

Fig. 14(b) shows the influence of blade length on the mixing time of EEM. The results show that the mixing time decreases with the increase of blade length. The main reason is that the increase of blade length enhances the stirring intensity of the blade on EEM and promotes the diffusion of the tracer. When the blade length is 35 mm, the mixing time of EEM is the shortest, about 5.2 s.

Fig. 14(c) shows the influence of the number of impeller layers on the mixing time of EEM. The results show that the increase of the number of impeller layers enhances axial mixing effect of EEM. The upper impeller stirs the tracer above the stirring tank more strongly, resulting in a rapid decrease in the mixing time of EEM with the increase of the number of impeller layers. When the number of layers is three, the mixing time of EEM is shortest, about 1.72 s.

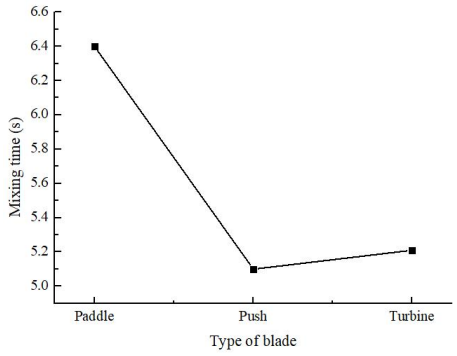

(a) different blade types

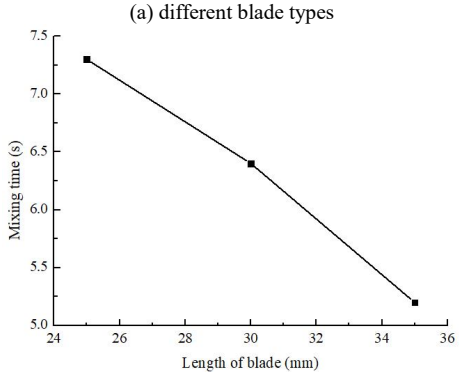

(b) different blade lengths

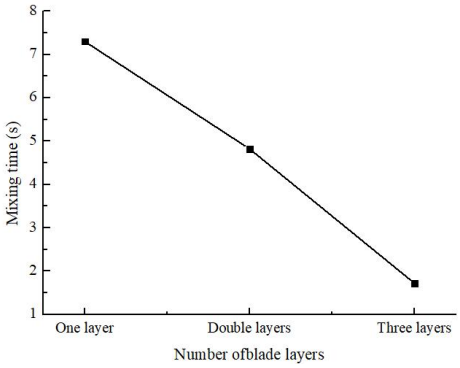

(c) different number of blade layers

Fig.14. Variation curve of mixing time under various working conditions

V. Conclusion

In this paper, numerical simulation research on the shear stirring of EEM was carried out using ANSYS-FLUNT fluid mechanics software. The effects of blade parameters (blade type, blade diameter, blade layer number, etc.) on the velocity field, shear rate, turbulent kinetic energy and homogeneity of EEM were analyzed. Through numerical simulation, the shear stirring parameters of EEM were optimized, and the following conclusions were drawn:

(1) The velocity distribution of EEM in the stirring tank is the greatest in the middle, followed by the bottom, and the least at the top. The turbine impeller has the greatest stirring and pushing effect on the EEM, followed by the push type, and the paddle type agitator has the least effect. With the increase of blade length and blade layer number, the shear mixing effect of the blade on EEM increases, and the turbulent range and flow velocity of EEM show an increasing trend.

(2) The shear rate of different blade types showed a trend of high in the middle and low on both sides at different heights. In the central region of the stirring tank, the shear rate of the turbine blade is the largest, followed by the blade blade and the propulsive type. At the bottom of the mixing tank, the shear rate of the push blade is the largest. With the increase of blade length, the eddy effect of the blade on the EEM near the wall of the mixing tank is gradually intensified, and the shear stress on the wall continues to increase, and the shear range correspondingly increases. In both the upper and lower regions of the stirred tank, the shear rate increased with the increase of the number of blade layers. For the middle region of the mixing tank, the shear rate of EEM of single blade is the largest.

(3) The results of the stirring and mixing time under different shear parameters show that the propeller blade has the best mixing effect, which can drive EEM to flow in the axial and radial directions, and its mixing time is the shortest at 5.1 s. The mixing time of EEM decreases with the increase of blade length, that is, the longer the blade length, the better the mixing effect, among which the mixing time of the 35 mm blade length is the shortest at 5.2 s. With the increase of blade layer number, the mixing time of EEM decreases, among which the three-layer stirring blade has the shortest mixing time at 1.72 s.

References

[1] P. Rueger and R. Calabrese, "Dispersion of water into oil in a rotor-stator mixer. Part 1: Drop breakup in dilute systems," *Chem. Eng. Res. Des*., vol. 91, no. 01, pp. 2122-2133, 2013.

[2] C. Kwon, K. Kim and U. Pak, "Effect of the stator tooth thickness on flow characteristics of high shear mixer," *Journal of Physics: Conference Series*., vol. 1750, no. 01, pp. 12-26, 2021.

[3] A. Gw, Y. Fan and W. Ke, "Estimation of the dissipation rate of turbulent kinetic energy: A review," *Chemical Engineering Science*., vol. 229, no. 01, pp. 116-133, 2020.

[4] A. Chang, H. Sun and K. Vafai, "Numerical analysis of flow and forced convection heat transfer of non-Newtonian fluid in a pipe based on fractional constitutive model," *International Journal of Numerical Methods for Heat and Fluid Flow*., vol. 31, no. 08, pp. 2680-2697, 2021.

[5] Z. Jianmin, W. Xuguang and G. Min, "The Effect of Shear Strength on Viscosity-Temperature Characteristics and Rheology Behavior of Emulsion Explosive Matrix," *Engineering Letter*., vol. 29, no. 03, pp. 1138-1142, 2021.

[6] C. Zhang, J. Gu and H. Qin, "CFD analysis of flow pattern and power consumption for viscous fluids in in-line high shear mixers," *Chem. Eng. Res. Des*., vol. 117, no. 01, pp. 190-204, 2017.

[7] H. Mortensen, F. Innings and A. Håkansson, "The effect of stator design on flowrate and velocity fields in a rotor-stator mixer-An experimental investigation," *Chem. Eng. Res. Des*., vol. 121, no. 01, pp. 245-254, 2017.

[8] C. Qin, C. Chen and Q. Xiao, "CFD-PBM simulation of droplets size distribution in rotor-stator mixing devices," *Chem. Eng. Sci*., vol. 155, no. 01, pp. 16-26, 2016.

[9] S. Wang, D. Luan and Y. Zhang, "Study on gas-liquid flow characteristics in stirred tank with dual- impeller based on CFD-PBM coupled model," *Chinese Journal of Chemical Engineering*., vol. 38, no. 01, pp. 63-75, 2021.

[10] W. Bujalski, Z. Jaworski and A. Nienow, "CFD study of homogenization with dual rushton turbines-comparison with experimental results: part I: initial studies," *Chemical Engineering Research & Design*., vol. 78, no. 01, pp. 327-333, 2002.

[11] K. Ng, N. Fentiman and K. Lee, "Assessment of sliding mesh CFD predictions and LDA measurements of the flow in a tank stirred by a rushton impeller," *Chemical Engineering Research & Design*., vol. 76, no. 06, pp. 737-747, 1998.

[12] P. Armenante, C. Luo and C. Chou, "Velocity profiles in a closed, unbaffled vessel: comparison between experimental LDV data and numerical CFD predictions," *Chemical Engineering Science*., vol. 52, no. 20, pp. 3483-3492, 1997.

[13] Wu, B., "CFD investigation of turbulence models for mechanical agitation of non-Newtonian fluids in anaerobic digesters," *Water Research*., vol. 45, no. 05, pp. 2082-2094, 2011.

[14] C. Nicholas and B. Reginald, "CFD simulation of solids suspension in mixing vessels," *The Canadian Journal of Chemical Engineering*., vol. 80, no. 04, pp. 721-726, 2002.

[15] F. Wang, M. Zaisha and X. Shen, "Numerical study of solid-liquid two-phase flow in stirred tanks with Rushton impeller - (II) Prediction of critical impeller speed," *Chinese J Chen Eng*., vol. 12, no. 05, pp. 605-609, 2004.

[16] Z. Jianmin, W. Xuguang and A. Huaming, "The Analysis of Blasting Seismic Wave Passing Through Cavity Based on SPH-FEM Couple Method," *Engineering Letter*., vol. 27, no. 01, pp. 114-119, 2019.

[17] G. Micale, G. Montante and F. Grisafi, " CFD simulation of particle distribution in stirred vessels," *Chemical Engineering Research & Design.*, vol. 78, no. 3, pp. 435-444, 2000.

[18] V. Alopaeus, J. Koskinen and K. Keskinen, "Simulation of the population balances for liquid-liquid systems in a nonideal stirred tank. Part 2-parameter fitting and the use of the multiblock model for dense dispersions," *Chemical Engineering Science.*, vol. 57, no. 10, pp. 1815-1825, 2002.